A&A 435, 1087–1097 (2005)
DOI: 10.1051/0004-6361:20041994

Astronomy & Astrophysics

Nebular abundances of southern symbiotic stars⋆,⋆⋆

G. J. M. Luna and R. D. D. Costa

Instituto de Astronomia, Geofisica e Ciências Atmosféricas (IAG), Universidade de São Paulo, São Paulo, Brazil
e-mail: [gjmluna;roberto]@astro.iag.usp.br

Received 10 September 2004 / Accepted 8 February 2005

Abstract. We have calculated relative element abundances for a sample of 43 symbiotic stars. Helium abundances and the relative elemental abundances N/O, Ne/O, Ar/O were derived from new spectra collected in the optical range through low dispersion spectroscopy. The He ionic abundances were derived taking into account self-absorption effects in Balmer lines. We found that the symbiotic stars in the galactic bulge have heavy element abundances showing the same wide distribution as other bulge objects. In the galactic disk, the symbiotic stars follow the abundance gradient as derived from different kinds of objects.

Key words. stars: binaries: symbiotic – stars: abundances – Galaxy: abundances

1. Introduction

Symbiotic stars are binary systems with large periods and strong interaction. There is an agreement in the fact that they consist of (at least) three components: a giant star, a hot source like a white dwarf, a main sequence star or even a neutron star (GX1+4), and a nebula ejected by the red giant, as was shown by Nussbaumer et al. (1988). The nebula can be ionized by the UV radiation from the hot source and in some eruptive symbiotic stars also by the region where the winds from the hot and cold sources collide (Willson et al. 1984). As the emission lines are very strong, the symbiotic stars are easily observable at large distances and are useful tools to test some aspects of the chemical composition of the low and intermediate mass population of the disk and galactic bulge as well as the evolution of double stars.

Some studies on nebular abundances in symbiotic stars have been performed in the optical region (see Costa & de Freitas Pacheco 1994; Pereira et al. 2002; Gutierrez Moreno & Moreno 1999) but with a small number of objects. Medina Tanco & Steiner (1995) have performed spectral classification of a sample of symbiotic stars toward the galactic bulge, but they did not derive chemical abundances. In the UV region, CNO abundances were derived for representative samples of symbiotics using IUE data (e.g. Nussbaumer et al. 1988; Schmid & Nussbaumer 1993).

The analysis of chemical abundances is required to investigate the surface enrichment of the red giant photosphere, whose stellar wind reflects the modifications introduced by dredge up processes during the stellar evolution. In this case, the investigation can be performed through techniques developed to study emission nebulae, which allow the determination of chemical abundances of elements such as helium, nitrogen, oxygen, neon and argon. Helium abundances must be derived with some caution, because the metastability of the 2^3S level causes radiative transfer effects and induces collisional excitation which can affect the final result. A second problem arises from the use of the Balmer decrement for reddening correction. The observed values suggest self-absorption effects in some systems which must be taken into account.

In this work we report the derivation of relative elemental abundances for 43 southern symbiotic stars. In Sects. 2 to 4 we discuss the observation and reduction techniques, in Sects. 5 to 7 the methods of analysis are described, and in Sect. 8 the results are discussed.

2. The sample

Our sample was selected from the Belckzyǹski et al. (2000) catalog of symbiotic stars, and one object (SS73 71) was added from Pereira et al. (2002). As a selection criterion we chose all the symbiotic stars toward the galactic bulge, which we have roughly defined as the region between $20° \le l \le 20°$ and $20° \le b \le 20°$. With these criteria our sample has 90 objects. We cannot ensure that all of them belong to the galactic bulge, because of the lack of good distances for the sample, but clearly all of them belong to the intermediate age population of the disk/bulge regions. Additionally, we have observed some other objects from the Belckzyǹski et al. (2000) catalog, that are out of our bulge definition.

⋆ Based on observations made at Observatório do Pico dos Dias / LNA (Brazil) and European Southern Observatory (Chile).

⋆⋆ Table 2 is only available in electronic form at http://www.edpsciences.org

Table 1. Log of the observations.

	Source	Date	Observatory		Source	Date	Observatory
1	K6-6	6/25/2003	LNA	32	Hen 2-379	6/24/2003	LNA
2	SS73 117	6/26/2003	LNA	33	V2905 Sgr	6/26/2003	LNA
3	SS73 141	6/26/2003	LNA	34	V4018 Sgr	6/07/2002	LNA
4	Th 3-29	6/23/2003	LNA	35	SS73 122	6/16/2002	LNA
5	H 1-25	6/13/2002	LNA	36	Ap 1-8	6/13/2002	LNA
6	Th 3-17	6/23/2003	LNA	37	V2506 Sgr	6/25/2003	LNA
7	Hen 3-1410	6/24/2003	LNA	38	Pt 1	6/15/2002	LNA
8	AS 210	8/10/2002	ESO	39	H 2-38	6/07/2002	LNA
		6/12/2002	LNA	40	V2756 Sgr	6/26/2003	LNA
9	H 2-5	6/12/2002	LNA	41	SS73 129	6/16/2002	LNA
10	H 1-36	6/13/2002	LNA	42	HD 319167	10/09/2002	ESO
11	UKS Ce 1	6/12/2002	LNA	43	V4074 Sgr	6/07/2002	LNA
12	HK Sco	6/14/2002	LNA	44	V3804 Sgr	6/14/2002	LNA
13	CL Sco	6/07/2002	LNA	45	Hen 3-1342	6/14/2002	LNA
14	WSTB 19W032	6/16/2002	LNA	46	AS 255	6/13/2002	LNA
15	Y CrA	6/13/2002	LNA	47	AS 269	10/08/2002	ESO
16	Hen 2-171	6/07/2002	LNA	48	SS 73 96	6/16/2002	LNA
17	AE Ara	6/12/2002	LNA	49	H 2-34	6/16/2002	LNA
18	V343 Ser	6/07/2002	LNA	50	SS73 71	10/10/2002	ESO
19	FN Sgr	6/07/2002	LNA	51	CD 43 -14304	6/23-24/2003	LNA
		6/23/2003	LNA	52	Hen 3-1761	6/23/2003	LNA
20	MWC 960	6/14/2002	LNA	53	R Arq	6/23/2003	LNA
21	RT Ser	6/07/2002	LNA	54	RR Tel	6/23/2003	LNA
22	MaC 1-9	6/16/2002	LNA	55	V919 Sgr	6/23/2003	LNA
23	UU Ser	6/25/2003	LNA	56	Hen 3-863	6/24/2003	LNA
24	V2601 Sgr	6/14/2002	LNA	57	LT Del	6/24/2003	LNA
25	V3811 Sgr	6/26/2003	LNA	58	WRAY 16 377	6/24/2003	LNA
26	ALS 2	6/24/2003	LNA	59	Bl 3-6	6/25/2003	LNA
27	V4141 Sgr	6/16/2002	LNA	60	SS73 29	6/25/2003	LNA
28	V2416 Sgr	6/07/2002	LNA	61	AG Peg	6/26/2003	LNA
29	M 1-21	6/26/2003	LNA	62	AS 327	6/26/2003	LNA
30	Hen 3-1591	6/14/2002	LNA	63	FG Ser	6/26/2003	LNA
		10/13/2002	ESO	64	PU Vul	6/26/2003	LNA
31	V2116 Oph	6/12/2002	LNA				

3. Observations

Spectroscopic observations were performed in two runs at the National Laboratory for Astrophysics (Brasópolis, MG, Brazil) from 7–16 Jun., 2002, and from 23–26 Jun., 2003, using a Boller & Chivens Cassegrain spectrograph attached to the 1.60 m telescope with a dispersion of 4.4 Å/pixel. Some observations were made at ESO using the 1.52 m telescope in La Silla, Chile (from 8–13 Oct., 2002) with a Boller & Chivens Cassegrain spectrograph with a dispersion of 2.2 Å/pixel. Spectra cover the range 3800–7400 Å. The log of the observations can be seen in Table 1. Each object was observed at least twice in the corresponding observational run, once with a short exposure time to get the fluxes of Hα, Hβ, Hγ and Hδ to derive the reddening correction, and again with a longer exposure time, saturating the Balmer lines and getting the weaker line fluxes. All the observations were performed in weather conditions compatible with flux calibration, and with an average seeing of 2 arcsec for LNA and 1 arcsec for ESO. Flux calibration for each object was secured through observations of standard stars on each night. Reduction was performed using the IRAF[1] package and followed the standard procedures, consisting of bias image subtraction, flat-fielding, wavelength and flux calibration. Figure 2 displays sample spectra for two objects, including the main diagnostic lines. Emission line fluxes were calculated by adopting Gaussian profiles; a Gaussian deblending routine was also used when necessary. Table 2, available electronically at the CDS, contains extinction-corrected fluxes in the Hβ = 100 scale for the objects of our sample. See Sect. 7.1 for a discussion of the accuracy of the results.

4. Reddening correction

In the low density limit, Balmer ratios can be used to derive interstellar extinction by comparing line ratios predicted by the recombination theory with the observed values, as described by Osterbrock (1989). It was already noticed that in symbiotic stars the Balmer ratios are far from the expected values resulting from interstellar extinction only (Costa & de Freitas Pacheco 1994). These deviations from Case-B can

[1] IRAF is distributed by the National Optical Astronomy Observatories, operated by AURA, Inc., under cooperative agreement with the NSF.

Article published by EDP Sciences and available at http://www.edpsciences.org/aa or http://dx.doi.org/10.1051/0004-6361:20041994

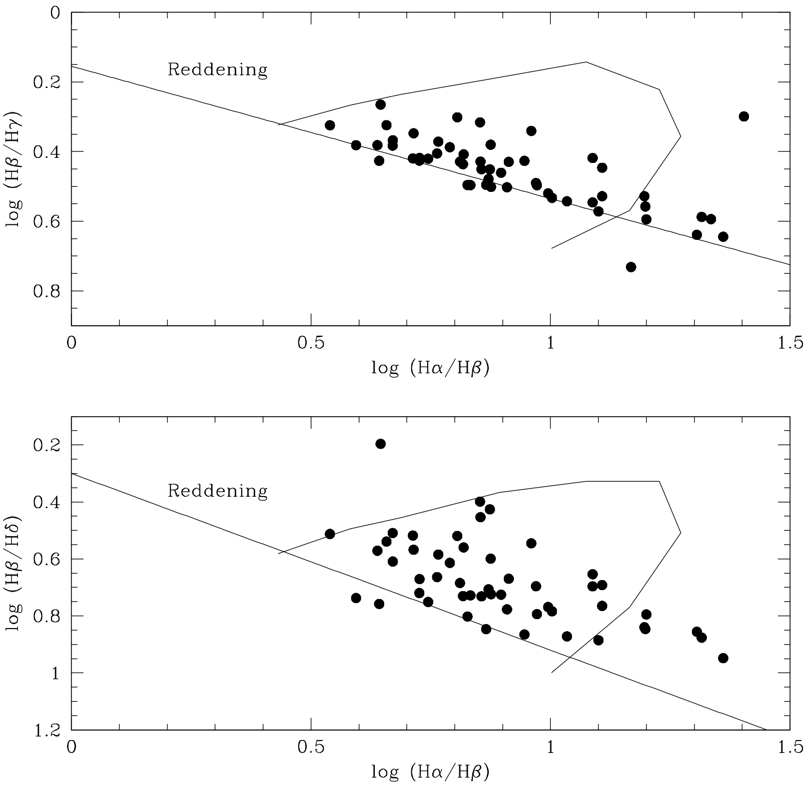

Fig. 1. $H\alpha/H\beta$ vs. $H\beta/H\gamma$ and $H\alpha/H\beta$ vs. $H\beta/H\delta$ for the objects of our sample. The figure has the same format as used by Netzer (1975), the curves are parametrized in $\tau_{H\alpha}$ values. We used only $\tau_\alpha = 10^6$ which correspond to optically thicker nebulae. For values of τ_α and $\tau_{H\alpha}$ see Netzer's (1975) Table 1.

be attributed to self-absorption effects, as described by Netzer (1975) for AGNs. Considering that symbiotic nebulae are very dense, optical depth effects should be present, therefore we adopted the Netzer (1975) and Almog & Netzer (1989) results for derivation of the reddening correction and HeI abundances.

Reddening correction was derived according to the procedure described by Gutiérrez-Moreno & Moreno (1996). This method simultaneously determines reddening and optical depth in $H\alpha$ using the Balmer decrement values computed by Netzer (1975) for different electron densities and different optical depths at $Ly\alpha$ (τ_α), under conditions of self-absorption. When using this procedure, we have adopted the interestellar absorption curve from Cardelli et al. (1989), and used Netzer's (1975) Balmer decrement values for $\log N_e = 8$.

Another direct graphical approach to the problem has been proposed (see for example Pereira 1995; Costa & de Freitas Pacheco 1994), resulting in similar values for the reddening correction. Figure 1 shows this method, displaying $H\alpha/H\beta$ vs. $H\beta/H\gamma$ and $H\alpha/H\beta$ vs. $H\beta/H\delta$ for the objects of our sample. The curves are parametrized in optical depth in $H\alpha$ ($\tau_{H\alpha}$), for $\tau_\alpha = 10^6$ which corresponds to optically thicker nebulae. The straight line indicates the reddening vector in both panels. Basically, the method consists of the determination of the $H\alpha/H\beta$ value that corresponds to the intersection of the object's reddening vector (parallel to the reddening vector in Fig. 1) and the τ_α curve. However, the graphical nature of this method can potentially lead to errors due to the limited sampling of the Balmer decrement computed by Netzer (1975), as can be seen in the figure.

In view of these limitations we adopted the analytical procedure described by Gutierrez-Moreno & Moreno (1996). A few objects in our sample have reddening values from the 2200 Å feature listed in Table 3, derived from IUE. We did not use these values in order to apply the same criteira for the reddening determination to the whole sample.

Nevertheless it should be noted that derivation of reddening correction for symbiotic stars can be performed using different techniques using their spectra, depending on the available spectral range and resolution, as pointed out by Mikolajewska et al. (1997), and the resulting values are usually quite different and dependent on the adopted method. The $E(B-V)$ values calculated for our sample and extracted from the literature are listed in Table 3.

Figure 2 displays spectra of two objects of our sample. The most important diagnostic lines are identified.

5. Physical conditions

The usual forbidden line ratios used to derive physical parameters of emission nebulae do not allow a unique electron temperature determination since the symbiotic nebula likely have a large density stratification. However the derivation of the ionic concentrations in the ionized gas requires previous knowledge of the electron temperature and density. From optical spectra

Table 3. N_e (cm^{-3}), $E(B-V)$ and $\tau_{H\alpha}$ derived for our sample.

	Source	$E(B-V)$	$\tau_{H\alpha}$	N_e[OIII]	Other $E(B-V)$
1	K6-6	2.23	15.4	5.29×10^6	
3	SS73 141[k]	0.55	1.3	1.0×10^8	
4	Th 3-29	1.77[b]	20.5	1.19×10^7	2.7[f]
5	H 1-25	2.54[b]	3.6	1.44×10^7	
7	Hen 3-1410	1.44[b]	9.7	8.73×10^6	
8	AS 210	0.49	4.3	3.87×10^6	≤0.5[c], 0.30 [d]
9	H 2-5	1.28	12.5	2.69×10^7	1.8[f]
10	H 1-36	0.51	1.4	4.92×10^5	0.71[d]
12	HK Sco	0.59	6.1	4.16×10^7	
13	CL Sco	0.22	6.4	3.67×10^7	0.2[e]
15	Y CrA	0.33	17.1	1.96×10^7	0.23[l]
16	Hen 2-171	0.59	2.9	2.66×10^6	0.58
17	AE Ara	0.14	5.6	1.53×10^7	0.5[f]
18	V343 Ser	1.18	8.5	1.19×10^7	
19	FN Sgr[g]	0.22	2.9	1.0×10^8	0.6[j]
20	MWC 960	0.84	4.9	1.63×10^7	0.7[j]
21	RT Ser[g]	1.08	10.8	1.0×10^8	
22	MaC 1-9[k]	1.14	4.72	1.0×10^8	1.2[f]
23	UU Ser	0.63	4.55	1.96×10^7	1.2[f]
24	V2601 Sgr	0.39	4.3	2.86×10^7	
26	ALS 2[g]	0.94	2.1	1.0×10^8	1.0[f]
27	V4141 Sgr	1.12	9.6	6.79×10^6	1.2[f]
28	V2416 Sgr	1.69	14.0	6.06×10^7	2.5[f]
29	M 1-21	0.88	5.5	1.0×10^8	1.0[f]
30	Hen 3-1591	0.06	19.0	1.1×10^7	
32	Hen 2-379	0.17	16.2	1.0×10^8	
33	V2905 Sgr	0.43	3.8	3.24×10^7	
34	V4018 Sgr	0.44	3.9	4.16×10^7	0.4[n]
35	SS73 122	0.84	9.9	4.38×10^6	0.92[a], 1.3[f]
36	Ap 1-8	1.04	3.6	4.12×10^6	0.6[f]
37	V2506 Sgr[k]	0.64	3.9	1.0×10^8	0.5[f]
38	Pt 1	0.95	8.9	4.17×10^7	
39	H 2-38	0.66	15	6.4×10^6	0.51[d], 1.2[f]
40	V2756 Sgr	0.32	8.75	1.05×10^7	0.0[f]
41	SS73 129[k]	0.78	3.4	1.0×10^8	1.6[f]
42	HD 319167	0.66	3.3	3.67×10^7	1.0[f]
44	V3804 Sgr	0.25	7.9	5.64×10^6	
45	Hen 3-1342	0.63	4.1	2.66×10^6	
46	AS 255[k]	0.68	8.0	1.0×10^8	
47	AS 269	2.08[b]	2.7	1.0×10^8	2.4[f]
48	SS 73 96	1.48	10.1	1.0×10^8	
49	H 2-34	1.29	11.7	1.05×10^7	
50	SS73 71	0.34	14.6	8.2×10^6	0.42[h]
51	CD 43 -14304[j]	0.76	3.0	1.0×10^8	≤0.2[c]
52	Hen 3-1761	0.15	12.6	1.4×10^7	
53	R Arq	0[i]	0	2.6×10^5	0.08[l]
54	RR Tel	0.05	4.3	4.67×10^6	0.09[l]
55	V919 Sgr[g]	0.38	10.3	1×10^8	
56	Hen 3-863	0.19	7.4	1.0×10^8	
57	LT Del[g]	0.41	...	1.0×10^8	
58	WRAY 16 377	0.83	1.15	2.09×10^7	
60	SS73 29	0.50	...	1.53×10^7	1.0[j]
61	AG Peg[k]	0.36	6.5	1.0×10^8	0.12[l]
62	AS 327[k]	0.86	5.4	1.0×10^8	1.1[f]
63	FG Ser	0.78	14.7	4.72×10^7	0.82[m]
64	PU Vul	0.29	6.8	1.53×10^7	

[a] Pereira (1995); [b] using Hα & Hγ; [c] Schmid & Nussbaumer (1993); [d] Pereira et al. (1998); [e] Michalitsianos et al. (1982); [f] Mikolajewska et al. (1997); [g] N_e assumed minimum value; [h] Pereira et al. (2002); [i] Simon (2003); [j] Munari & Buson (1994); [k] without diagnostic lines, $N_e = 10^8$; [l] Nussbaumer et al. (1988); [m] Gutiérrez-Moreno et al. (1992); [n] Munari & Buson (1993).

these parameters can usually be estimated from line intensity ratios such as, among others:

$$R([\mathrm{OIII}]) = \frac{\lambda 5007 + \lambda 4959}{\lambda 4363} \quad (1)$$

$$R([\mathrm{NII}]) = \frac{\lambda 6584 + \lambda 6548}{\lambda 5755} \quad (2)$$

$$R([\mathrm{SII}]) = \frac{\lambda 6717}{\lambda 6730}. \quad (3)$$

In view of the high density of symbiotic nebulae it is difficult to use the R(SII) to estimate the electron density, as this relation produces unique results for $N_e \leq 10^5$ (Osterbrock 1989). We estimated a lower limit for the density from the R([OIII]) and R([NII]) ratios assuming $T_e \approx 12\,000$ K, which is an acceptable value for symbiotics (Nussbaumer et al. 1988), and adopted two different density zones, namely N_e[OIII] and N_e[NII], for those objects where both ratios were available. Otherwise a single zone was assumed. Figure 3 displays an example of the behavior of R([OIII]) and R([NII]) for Hen 2-171.

R([NII]) and R([OIII]) characterize two distinct regions above which the relations are sensitive to density, resulting in lower limits for this parameter. This picture is clearly an oversimplification of the true situation, however, high resolution IUE spectra of V 1016 Cyg suggest an interpretation not inconsistent with such an approximation (Deuel & Nussbaumer 1984). Narrow and broad components suggesting at least two regions with distinct densities are also seen in Coudé spectra of HM Sge (Stauffer 1984). We consider that in the R([NII]) region the main ionic species are N^+, O^+, S^+, while in the R([OIII]) region species of higher excitation like O^{+2}, S^{+2}, Ne^{+2}, Ar^{+2}, Ar^{+3} are dominant. Only in AS 210, RR Tel, PN H 1-36, PN H 2-38 and Hen 2-171 were both density regions used. For these objects, R([NII]) lead to density values (in cm^{-3}) of respectively : 2.6×10^5, 3.38×10^5, 1.03×10^5, 3.38×10^5, $1. \times 10^5$. The derived values for N_e are listed in Table 3.

6. Helium abundance

Helium abundance is a key parameter to characterize chemical evolution either of stars and galaxies. As discussed by Clegg (1987), line formation in HeI is complex in view of the metastability of the lowest triplet level, which can cause some lines to

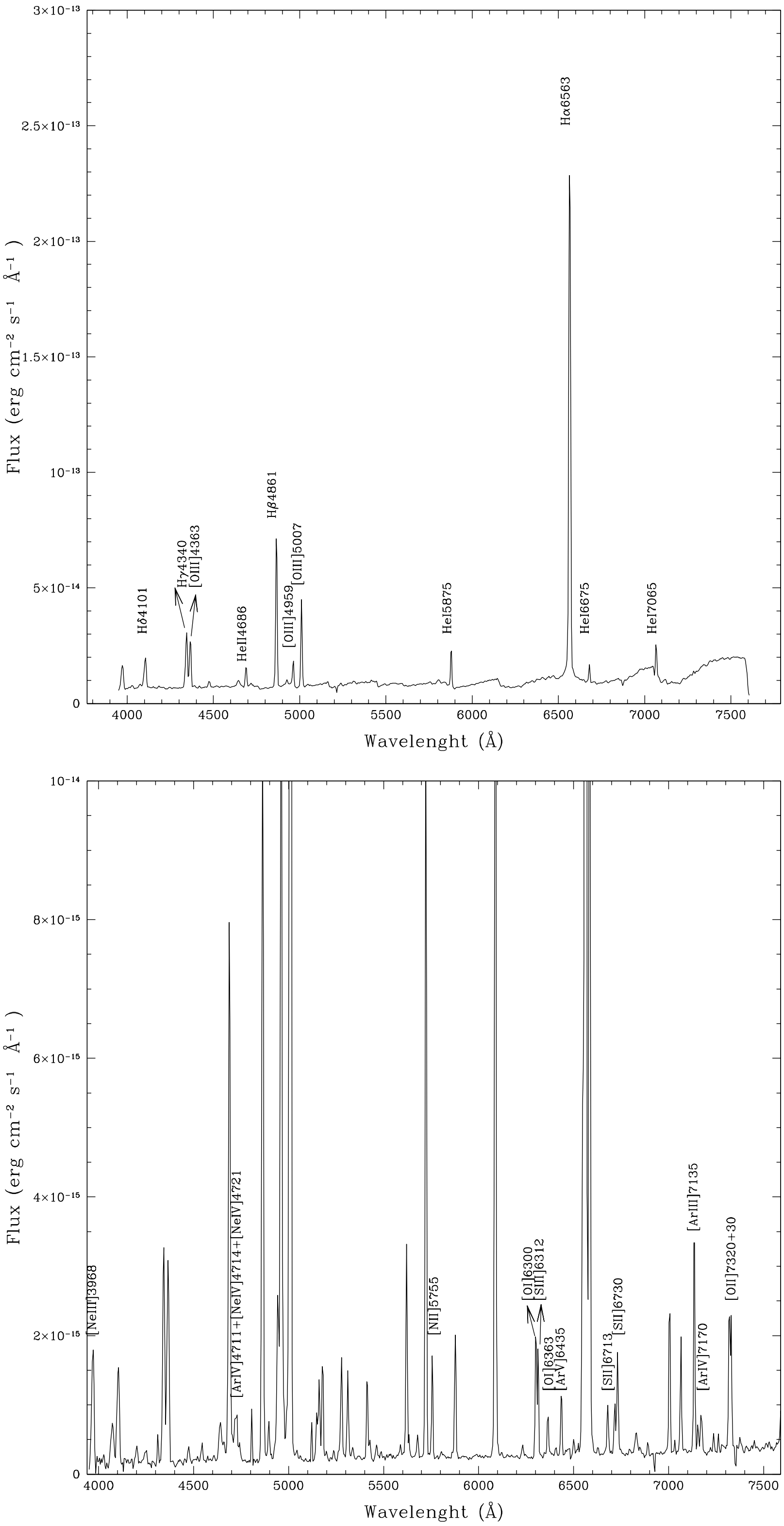

Fig. 2. Diagnostic lines in the spectra of Hen 2-171 (*lower*) and CL Sco (*upper*).

become optically thick. In particular, the collisional enhancement of HeI lines from the metastable 2^3S level is an important issue that cannot be excluded, as indicated by Kingdon & Ferland (1995). This is a specially controversial subject in symbiotic stars in view of their high nebular densities.

Usually helium abundance is expressed relative to hydrogen. As discussed in Sect. 4, in high density nebulae self-absorption effects are present in the Balmer series. In order to minimize these effects on the helium abundance, Schmid & Schild (1990) used the ratio between HeII and higher

Article published by EDP Sciences and available at http://www.edpsciences.org/aa or http://dx.doi.org/10.1051/0004-6361:20041994

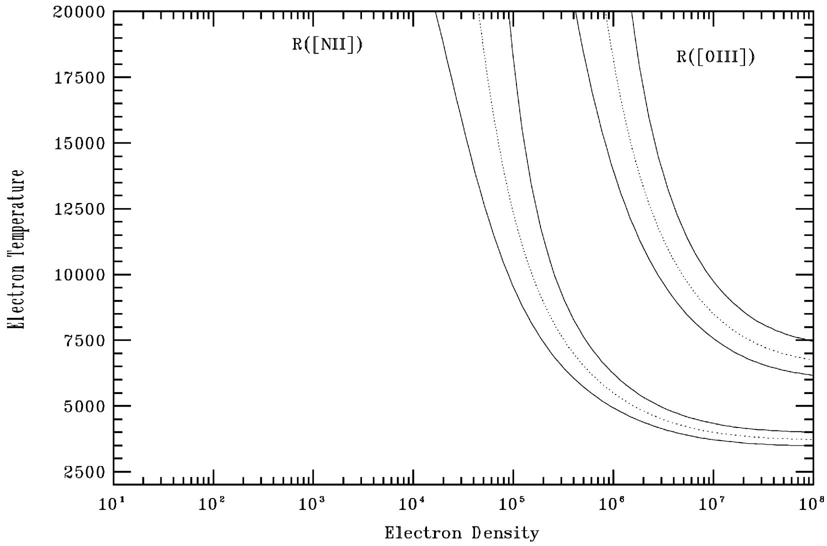

Fig. 3. Behavior of R([OIII]) and R([NII]) relations for Hen 2-171. The solid lines represent an uncertainty of 2σ with respect to the calculated value.

excitation Balmer lines when deriving the final helium abundance. Here we adopted a similar procedure, taking Hγ as our reference line. It was chosen as a compromise between lower lines, more affected by self absorption effects, and higher, weaker, lines. The optical depth in this line can be scaled to the value of $\tau_{\mathrm{H}\alpha}$. Using the optical depth in Hα, $\tau_{\mathrm{H}\alpha}$, which is derived from our reddening calculation, the optical depth in Hγ, $\tau_{\mathrm{H}\gamma}$ is $0.07 \times \tau_{\mathrm{H}\alpha}$. In the cases that $\tau_{\mathrm{H}\gamma} \leq 0.5$ we would expect that self-absorption effects are negligible and no large errors are being committed.

The HeI abundances were computed considering the possibility of large collisional excitation and self absorption effects, following the procedure described in detail by Costa & de Freitas Pacheco (1994). In the present work we derived the abundance from lines λ5876 and λ7065, weighted by their intensities. Line λ6678 was not used to compute HeI abundance because we have detected that in many objects it is placed over the wings of Hα, resulting in overestimated fluxes. Line λ7065 was also used to estimate the optical depth in λ3889 ($\tau_{(\lambda 3889)}$) since this optical depth is required to derive emissivities calculated by Almog & Netzer (1989) for HeI lines. The concentration of He^+ can consequently be obtained from the relation (de Freitas Pacheco & Costa 1992):

$$\frac{n(\mathrm{He}^+)}{n(\mathrm{H})} = \frac{5.9}{E_\lambda(\tau)} \frac{I_\lambda}{I_\gamma} \tag{4}$$

where I_λ/I_γ is the line intensity ratio between the considered HeI line and Hγ and $E_\lambda(\tau)$ is the emissivity calculated by Almog & Netzer (1989) (see their Table 2) as a function of $\tau(\lambda 3889)$. As pointed by de Freitas Pacheco & Costa (1992), the intensity of the HeIλ7065 line in RR Tel is too high and produces unrealistic values for $\tau(\lambda 3889)$ and therefore higher HeI abundance. Table 4 shows the resulting He^+ abundances together with the He^{+2} derived using the λ4686 line.

7. Abundances of heavy elements

In order to minimize the effects of self-absorption in Balmer lines on the derived abundances, we calculated elemental ratios with respect to oxygen, since they can be derived directly from forbidden transitions. In the R(NII) region we derive the nitrogen to oxygen ratio from the relation

$$\frac{\mathrm{N}}{\mathrm{O}} \approx \frac{\mathrm{N}^+}{\mathrm{O}^+}. \tag{5}$$

In the R([OIII]) region, the relative abundances of neon and argon with respect to oxygen can be obtained from Schmid & Schild (1990):

$$\frac{\mathrm{Ne}}{\mathrm{O}} \approx \frac{\mathrm{Ne}^{+2}}{\mathrm{O}^{+2}} \tag{6}$$

$$\frac{\mathrm{Ar}}{\mathrm{O}} \approx \frac{\mathrm{Ar}^{+2} + \mathrm{Ar}^{+3}}{\mathrm{O}^{+2}}. \tag{7}$$

To derive the ion concentrations we have adopted a five level atom model, including collisional excitation and desexcitation and radiative transitions in the statistical balance equations. The model is described by Shaw & Dufour (1994), and the relevant atomic data used can be retrieved directly from IRAF *nebular* package

Relative elemental abundances of heavier elements can be derived from emission lines which originate from a common region. In dense nebulae, the ionization structure of helium is particularly well defined by the Strömgren radii of He^{+2} and H^+. It is therefore appropriate to compare ions that coincide with either the He^{+2} or He^+ regions. With our spectral resolution, we can identify in some objects two different density regions, one for the N^+ and the other for O^{+2}, therefore as was pointed earlier we calculate relative elemental abundances for ions formed in the same density region.

The N^+ abundance was derived from λ6548+84 and/or λ5755, and O^+ was derived from λ7320+30 lines. For the O^{+2} abundance we have used a mean value between

Table 4. He abundances.

	Source	He I	He II	He		Source	He I	He II	He
1	K6-6	0.232	0.033	0.265	35	SS73 122	0.177	0.048	0.225
5	H 1-25	...	...	...	36	Ap 1-8	0.113	0.068	0.181
7	Hen 3-1410	0.191	0.047	0.238	37	V2506 Sgr	...	...	...
8	AS 210	0.029	0.058	0.087	38	Pt 1	...	...	...
10	H 1-36	0.057	0.054	0.111	39	H 2-38	0.129	0.068	0.197
12	HK Sco	0.083	0.088	0.171	40	V2756 Sgr	0.177	0.071	0.248
13	CL Sco	0.110	0.013	0.123	42	HD 319167	0.093	0.009	0.102
15	Y CrA	0.115	0.017	0.132	44	V3804 Sgr	0.207	0.014	0.221
16	Hen 2-171	0.063	0.074	0.137	45	Hen 3-1342	0.167	0.053	0.220
17	AE Ara	0.141	0.013	0.54	46	AS 255	0.179	0.092	0.271
18	V343 Ser	...	...	...	50	SS 73 71	0.182	0.038	0.220
19	FN Sgr	0.099	0.082	0.181	51	CD 43 -14304	0.134	0.059	0.193
20	MWC 960	0.127	0.061	0.188	52	Hen 3-1761	0.217	0.048	0.265
21	RT Ser	...	...	...	53	RR Tel	...	...	...
23	UU Ser	0.102	0.048	0.15	55	V919 Sgr	0.126	0.041	0.167
24	V2601 Sgr	0.122	0.025	0.147	56	Hen 3-863	0.098	0.052	0.150
26	ALS 2	0.096	0.050	0.146	57	LT Del	0.113	0.020	0.133
27	V4141 Sgr	0.179	0.006	0.185	58	WRAY 16 377	...	...	...
28	V2416 Sgr	0.084	0.070	0.154	61	AG Peg	0.128	0.087	0.215
29	M 1-21	0.093	0.040	0.133	62	AS 327	0.163	0.083	0.246
33	V2905 Sgr	0.168	0.006	0.174	64	PU Vul	0.083	0.063	0.146
34	V4018 Sgr	0.121	0.043	0.164					

[OIII]λ4363, [OIII]λ4959 and [OIII]λ5007, weighted by their intensities, and for Ne^{+2} we have used the [NeIII]λ3869 line when available, or [NeIII]λ3968. In almost all the sample, the dependence of the Ne/O relation to N_c (critical density) for the used lines is not very large, because the densities are similar or greater than N_c (Schmid & Schild 1990). The [ArIII]λ7136 and [ArIV]λ4740 lines were used together with [OIII] abundance for the Ar/O determination; the [ArIII]λ4711 line cannot be used because at our spectral resolution it was blended with [NeIV]λ4714. The ionic abundances were calculated with the task *nebular/abund* of IRAF and are listed in Table 5. They were calculated adopting T_e = 12 000 K and taking N_e from Table 3. The derived relative elemental abundances are listed in Table 6.

7.1. Precision of the abundance determination

Abundance determination involves many sources of errors like accuracy of the fluxes, limited precision in data reduction, uncertainties in reddening and the derived physical parameters, as well as in the adopted methodology to derive abundances. We tested the sensitivity of the abundances to the line fluxes for each object by calculating the mean and standard deviation for all the flux measurements of each spectral line for each object. The results can be seen in Fig. 4, where ΔF represents the standard deviation for each line. The points that form a straight line correspond to those lines for which we have only one measurement; for them we adopt an error of 30% for the lines weaker than (1/3)Hβ and 10% for the stronger lines (respect to Hβ = 100). The flux dispersions result in abundance dispersions that have a mean value of 0.2 dex for stronger lines such as [OIII], and 0.4 dex for weaker lines such as [ArIV], [NeIII], etc. These uncertainties are typical in this type of calculation (e.g. Escudero & Costa 2001).

We also tested the dependence of the derived abundances on $E(B-V)$, the most uncertain parameter in the process. As described in Sect. 4, we calculate $E(B-V)$ using the method described by Gutiérrez Moreno & Moreno (1996). To check the dependence of the derived relative abundances on the reddening, we considered an uncertainty of 50% in $E(B-V)$ and rederived the electron densities and abundances, which resulted in upper and lower limits of precision for our results. These limits are displayed in Fig. 5 as a mean error bar for the results. It can be seen that even such a large error in reddening does not affect our main conclusions.

8. Results and discussion

Our sample contains 54 objects for which ionic abundances have been derived. For many of them, these are the first abundances published. These abundances are similar to those obtained for nebulae that present similar spectroscopic behavior to planetary nebulae.

To perform the chemical diagnosis we have chosen emission lines from elements with similar ionization potentials, in order to minimize the effects of density gradients. We have obtained abundances ratios from collisionally excited lines, namely N/O, Ne/O and Ar/O.

We present the ionic concentrations for O, N, Ar, S, He and Ne. The relative elemental abundances show the composition of the interstellar medium at the time of progenitor formation, and the N and He abundances reflect the evolutionary state of the stars, showing that this class of objects have experienced dredge-up episodes, even up to the second one. Also the He and

Article published by EDP Sciences and available at http://www.edpsciences.org/aa or http://dx.doi.org/10.1051/0004-6361:20041994

Table 5. Ionic abundances for symbiotic stars in our sample.

Source	NII	OI	OII	OIII	NeIII	NeIV	SIII	ArV	ArIII	ArIV	NI
AE Ara	3.933×10^{-6}	2.157×10^{-5}	3.330×10^{-5}	1.470×10^{-4}	2.276×10^{-5}	2.665×10^{-5}	1.611×10^{-6}	3.417×10^{-6}	...	...	...
Ap 1-8	3.417×10^{-6}	...	...	1.302×10^{-5}	...	...	...	1.787×10^{-7}	1.357×10^{-8}	2.018×10^{-5}	...
AG Peg	1.024×10^{-4}	...	2.353×10^{-4}	4.000×10^{-4}	1.897×10^{-5}	...	...	...	...	...	0.05983
ALS 2	2.478×10^{-4}	...	2.622×10^{-4}	7.506×10^{-5}	7.235×10^{-5}	...	...	...	...	0.001206	...
AS 210	1.605×10^{-6}	2.669×10^{-6}	1.754×10^{-6}	1.295×10^{-4}	9.575×10^{-6}	5.862×10^{-5}	1.274×10^{-6}	2.078×10^{-7}	1.861×10^{-7}	2.346×10^{-7}	...
AS 255	...	2.971×10^{-4}	1.263×10^{-4}	5.101×10^{-5}	...	...	...	...	6.565×10^{-6}	9.061×10^{-5}	...
AS 327	4.596×10^{-5}	...	1.081×10^{-4}	1.626×10^{-4}	...	...	...	...	...	8.546×10^{-4}	...
CD 43 -14304	4.313×10^{-6}	...	4.059×10^{-5}	2.382×10^{-4}	2.104×10^{-5}	...	...	...	2.930×10^{-7}	3.232×10^{-4}	0.02439
CL Sco	1.384×10^{-5}	1.336×10^{-5}	...	5.814×10^{-4}	9.356×10^{-5}	8.066×10^{-5}	1.594×10^{-6}	1.273×10^{-6}	1.829×10^{-7}	1.450×10^{-5}	0.007804
FG Ser	1.087×10^{-4}	...	3.754×10^{-4}	2.514×10^{-4}	1.955×10^{-5}	...	...	...	...	5.659×10^{-4}	...
FN Sgr	6.043×10^{-5}	...	6.566×10^{-5}	2.622×10^{-4}	4.551×10^{-5}	...	5.739×10^{-6}	7.061×10^{-6}	...	8.320×10^{-4}	0.01075
H 1-25	2.256×10^{-4}	4.145×10^{-5}	1.699×10^{-6}	2.061×10^{-4}	...	...	...	...	8.756×10^{-8}	2.783×10^{-7}	...
H 1-36	2.495×10^{-5}	3.449×10^{-5}	3.447×10^{-5}	5.114×10^{-4}	6.280×10^{-5}	2.776×10^{-4}	7.722×10^{-6}	8.726×10^{-7}	1.535×10^{-6}	4.216×10^{-6}	...
H 2-34	3.240×10^{-6}	2.503×10^{-5}	5.670×10^{-6}	1.754×10^{-4}	...	...	4.097×10^{-6}	8.995×10^{-7}	1.259×10^{-7}	5.957×10^{-6}	0.003656
H 2-38	7.662×10^{-6}	1.794×10^{-5}	1.185×10^{-5}	9.006×10^{-4}	7.150×10^{-5}	1.842×10^{-4}	3.686×10^{-6}	1.257×10^{-6}	4.284×10^{-7}	2.727×10^{-6}	...
H 2-5	...	9.349×10^{-5}	...	2.950×10^{-4}	...	...	3.662×10^{-6}	2.713×10^{-6}	...	...	...
HD 319167	1.899×10^{-6}	1.640×10^{-5}	4.561×10^{-6}	1.838×10^{-4}	2.872×10^{-5}	5.349×10^{-5}	1.994×10^{-7}	4.307×10^{-7}	5.559×10^{-8}	2.977×10^{-6}	...
Hen 2-171	1.985×10^{-5}	9.651×10^{-6}	8.123×10^{-6}	3.409×10^{-4}	3.459×10^{-5}	1.796×10^{-4}	5.365×10^{-6}	1.155×10^{-6}	1.062×10^{-6}	2.068×10^{-6}	...
Hen 2-379	0.07021	...	...	0.001018	...	0.001649	...	...	...	...	...
Hen 3-1342	...	1.485×10^{-5}	6.465×10^{-6}	1.094×10^{-5}	...	...	3.548×10^{-6}	4.772×10^{-7}	2.308×10^{-7}	5.684×10^{-7}	...
Hen 3-1410	4.200×10^{-6}	...	8.082×10^{-6}	1.097×10^{-4}	...	...	...	4.579×10^{-7}	...	...	...
Hen 3-1591	3.998×10^{-4}	1.527×10^{-4}	1.201×10^{-4}	0.001048	9.513×10^{-5}	...	3.787×10^{-6}	8.230×10^{-7}	3.029×10^{-6}	3.165×10^{-5}	...
Hen 3-1761	1.113×10^{-4}	...	2.676×10^{-4}	3.304×10^{-4}	4.483×10^{-5}	1.684×10^{-4}	...	...	...	1.967×10^{-4}	...
Hen 3-863	...	...	2.380×10^{-4}	3.820×10^{-4}	9.932×10^{-6}	...	...	...	...	5.861×10^{-5}	0.1261
HK Sco	3.364×10^{-5}	...	3.423×10^{-5}	7.033×10^{-5}	4.788×10^{-6}	...	...	3.502×10^{-6}	...	6.584×10^{-5}	...
K6-6	3.446×10^{-6}	2.182×10^{-5}	4.302×10^{-6}	1.110×10^{-4}	...	7.921×10^{-5}	1.061×10^{-6}	3.094×10^{-7}	3.232×10^{-8}	4.675×10^{-5}	...
LT Del	4.330×10^{-5}	...	...	2.524×10^{-5}	...	...	...	...	...	6.490×10^{-4}	...
M1 -21	...	6.010×10^{-5}	1.750×10^{-5}	...	...	1.694×10^{-4}	2.847×10^{-6}	1.900×10^{-6}	...	2.342×10^{-4}	...
MaC 1-9	3.084×10^{-5}	...	3.464×10^{-5}	1.852×10^{-4}	...	...	...	...	...	...	...
MWC 960	4.429×10^{-6}	3.222×10^{-5}	8.880×10^{-6}	2.070×10^{-5}	...	...	2.093×10^{-6}	6.349×10^{-7}	...	8.069×10^{-6}	...
PN Pt 1	2.048×10^{-5}	3.606×10^{-4}	5.539×10^{-5}	8.610×10^{-5}	...	...	...	4.005×10^{-6}	...	...	...

Table 5. continued.

Source	NII	OI	OII	OIII	NeIII	NeIV	SIII	ArV	ArIII	ArIV	NI
PU Vul	2.173×10^{-5}	4.032×10^{-5}	1.124×10^{-5}	3.004×10^{-4}	8.958×10^{-5}	1.508×10^{-4}	2.329×10^{-6}	8.126×10^{-7}	3.322×10^{-7}	3.522×10^{-6}	8.831×10^{-4}
RR Tel	4.075×10^{-6}	6.376×10^{-6}	1.343×10^{-5}	2.577×10^{-4}	3.697×10^{-5}	3.280×10^{-4}	1.723×10^{-6}	6.723×10^{-7}	4.959×10^{-7}	2.975×10^{-6}	...
RT Ser	2.248×10^{-5}	3.522×10^{-4}	...	1.001×10^{-4}	...	1.508×10^{-4}	6.194×10^{-6}	...	...	...	8.145×10^{-4}
SS73 122	9.189×10^{-6}	2.258×10^{-5}	1.121×10^{-5}	1.805×10^{-4}	1.309×10^{-5}	5.898×10^{-6}	3.025×10^{-6}	6.724×10^{-7}	4.608×10^{-7}	2.546×10^{-6}	...
SS73 129	...	...	1.595×10^{-4}	2.415×10^{-4}	...	...	...	...	...	...	...
SS73 141	...	1.324×10^{-4}	...	...	...	...	...	3.145×10^{-6}	...	...	...
SS73 29	8.416×10^{-7}	...	...	3.885×10^{-5}	...	...	...	...	1.465×10^{-7}	...	...
SS73 71	5.180×10^{-6}	1.486×10^{-5}	...	1.007×10^{-4}	1.916×10^{-5}	4.335×10^{-5}	1.525×10^{-6}	7.450×10^{-7}	1.098×10^{-8}	1.060×10^{-5}	...
SS73 96	1.013×10^{-5}	1.129×10^{-5}	2.122×10^{-5}	1.506×10^{-4}	5.674×10^{-6}	1.923×10^{-4}	3.247×10^{-6}	1.551×10^{-6}	1.802×10^{-8}	8.404×10^{-6}	...
Th 3-29	...	4.277×10^{-5}	1.271×10^{-5}	1.504×10^{-4}	...	...	...	...	1.908×10^{-7}	1.859×10^{-6}	...
UU Ser	5.009×10^{-6}	...	...	3.773×10^{-5}	...	...	...	...	...	...	0.002409
V2416 Sgr	7.463×10^{-6}	1.576×10^{-4}	9.246×10^{-7}	8.516×10^{-5}	5.861×10^{-6}	...	5.966×10^{-6}	3.397×10^{-6}	8.160×10^{-9}	1.168×10^{-7}	6.465×10^{-5}
V2506 Sgr	...	...	...	...	...	...	...	...	...	...	...
V2601 Sgr	1.678×10^{-5}	1.770×10^{-5}	1.230×10^{-5}	5.759×10^{-5}	1.169×10^{-5}	2.135×10^{-5}	4.774×10^{-6}	4.048×10^{-6}	...	...	...
V2756 Sgr	2.773×10^{-6}	6.385×10^{-6}	2.903×10^{-5}	1.609×10^{-4}	...	7.063×10^{-5}	...	7.047×10^{-7}	5.654×10^{-7}	...	0.002434
V2905 Sgr	...	...	7.786×10^{-5}	3.812×10^{-4}	3.743×10^{-5}	...	...	...	...	1.902×10^{-4}	...
V343 Ser	1.368×10^{-6}	...	9.453×10^{-7}	2.570×10^{-5}	...	...	4.584×10^{-8}	1.283×10^{-6}	...	2.078×10^{-8}	6.240×10^{-6}
V3804 Sgr	4.426×10^{-6}	2.158×10^{-5}	1.026×10^{-5}	1.198×10^{-4}	2.214×10^{-5}	...	2.639×10^{-6}	1.426×10^{-6}	4.156×10^{-7}	1.139×10^{-6}	...
V4018 Sgr	1.399×10^{-5}	...	9.158×10^{-6}	1.022×10^{-4}	9.888×10^{-6}	1.013×10^{-4}	...	1.998×10^{-6}	...	...	0.002753
V4141	4.566×10^{-6}	1.154×10^{-5}	3.239×10^{-6}	2.173×10^{-4}	1.744×10^{-5}	2.562×10^{-5}	1.422×10^{-6}	4.299×10^{-7}	3.017×10^{-7}	1.828×10^{-6}	0.001029
V919 Sgr	9.766×10^{-5}	...	4.403×10^{-4}	3.969×10^{-4}	8.841×10^{-5}	5.536×10^{-4}	...	...	...	6.609×10^{-4}	0.03935
WRAY 16 377	5.147×10^{-6}	...	3.001×10^{-5}	1.593×10^{-4}	1.230×10^{-5}	...	...	...	7.878×10^{-8}	1.332×10^{-4}	...
Y Cra	...	9.477×10^{-5}	...	2.525×10^{-4}	3.029×10^{-5}	2.976×10^{-4}	5.461×10^{-6}	...	9.731×10^{-8}	1.408×10^{-4}	...

Table 6. Relative elemental abundances.

	Source	N/O	Ne/O	Ar/O		Source	N/O	Ne/O	Ar/O
1	K6-6	0.801	...	0.421	34	V4018 Sgr	1.527	0.097	...
4	Th 3-29	...	...	0.014	35	SS73 122	0.820	0.072	0.017
5	H 1-25	...	...	0.002	38	Pt 1	0.369	...	...
7	Hen 3-1410	0.519	...	...	39	H 2-38	0.646	0.079	0.003
8	AS 210	0.915	0.074	0.003	40	V2756 Sgr	0.095	...	...
10	H 1-36	0.724	0.123	0.011	42	HD 319167	0.416	0.156	0.016
12	HK Sco	0.982	0.068	...	44	V3804 Sgr	0.431	0.185	0.013
13	CL Sco	...	0.161	0.025	45	Hen 3-1342	...	...	0.073
15	Y CrA	...	0.119	0.558	48	SS73 96	0.477	0.037	0.056
16	Hen 2-171	2.443	0.101	0.009	49	H 2-34	0.571	...	0.035
17	AE Ara	0.118	0.155	...	50	SS 73 71	...	0.190	0.105
18	V343 Ser	1.447	...	...	51	CD 43 -14304	0.106	0.088	...
19	FN Sgr	0.920	0.173	...	52	Hen 3-1761	0.416	0.136	...
20	MWC 960	0.499	...	...	53	RR Tel	0.303	0.143	0.013
22	MaC 1-9	0.890	...	...	55	V919 Sgr	0.222	0.222	...
24	V2601 Sgr	1.364	0.203	...	56	Hen 3-863	...	0.026	...
26	ALS 2	0.945	0.963	...	58	WRAY 16 377	0.171	0.077	0.836
27	V4141 Sgr	1.409	0.080	0.010	61	AG Peg	0.435	0.047	...
28	V2416 Sgr	...	0.069	0.001	62	AS 327	0.425	...	...
30	Hen 3-1591	3.329	0.090	0.033	63	FG Ser	0.289	0.077	...
33	V2905 Sgr	...	0.098	...	64	PU Vul	1.931	0.298	0.013

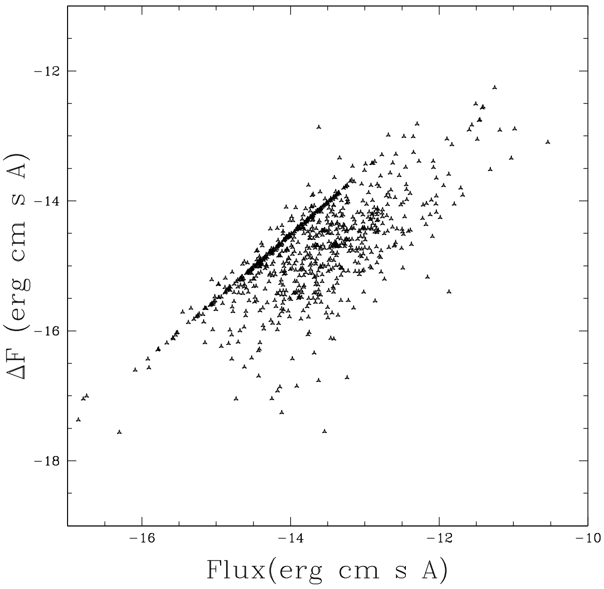

Fig. 4. Flux mean values vs. standard deviation (ΔF) from all the lines for each object of the sample.

N abundances are comparable with progenitors between 0.6 to 1.5 $M_{\odot}$.

Figure 5 shows the relation between N/O and He/H; as nitrogen and helium are nucleosynthesis products and related to the mass spectrum of the progenitors, they are expected to be correlated, therefore this relationship is important to the diagnosis of abundances. The figure combines data from symbiotics with other data from planetary nebulae (Escudero & Costa 2001; Escudero et al. 2004; Exter et al. 2004). It can be seen that the objects in this figure are distributed in two groups: a larger, upper group for which the planetary nebulae sample define a reasonably well-defined correlation between

Table 7. Mean Ne/O ratios for different samples.

Sample	Ne/O	Source
Bulge PNe	0.168 ± 0.070	Escudero et al. (2004)
Disk PNe	0.181 ± 0.129	Maciel & Köppen (1994)
Disk and Bulge PNe	0.223 ± 0.085	Exter et al. (2004)
This sample	0.154 ± 0.034	

log (He/H) and log (N/O), in the sense that helium-rich objects are usually nitrogen-rich. The symbiotic stars fit into this distribution, in spite of their dispersion. This correlation reflects the mass spectrum of the progenitors. A small group of PNe can also be seen with low log (N/O) and log (He/H) varying from –1.1 to –0.7. The same pattern appears in the results of Cuisinier et al. (1996) for galactic PNe and can be related to objects at high Z above the galactic plane. However, the uncertainties in distances, both for symbiotics and PNe, make this point still an open question.

The same figure also includes a model from Marigo (2001), with mixing-length parameter = 1.68 and initial metallicity $Z = 0.019$ and $Y = 0.273$, computed to $0.1026 \geq \mathrm{He} \geq 0.1387$ and $-0.9 \geq \log(\mathrm{N/O}) \geq -0.001$. Clearly, the dispersion of the data is high, but the model trend agrees with the mean values and tendencies for most of the PNe sample. For some symbiotic stars, however, this agreement cannot be seen, may be due to the uncertanties in the method used to derive He abundances and/or to Marigo's model that was produced for isolated stars, and some discrepacies are expected with respect to binary objects like symbiotics.

Nebular abundances of symbiotics should reflect the abundances of the intermediate mass stars from which they originate, irrespective of their position in the galaxy. To verify this behavior we compare the mean values of the Ne/O ratio for our sample of symbiotics to other samples of disk and bulge PNe.

Article published by EDP Sciences and available at http://www.edpsciences.org/aa or http://dx.doi.org/10.1051/0004-6361:20041994

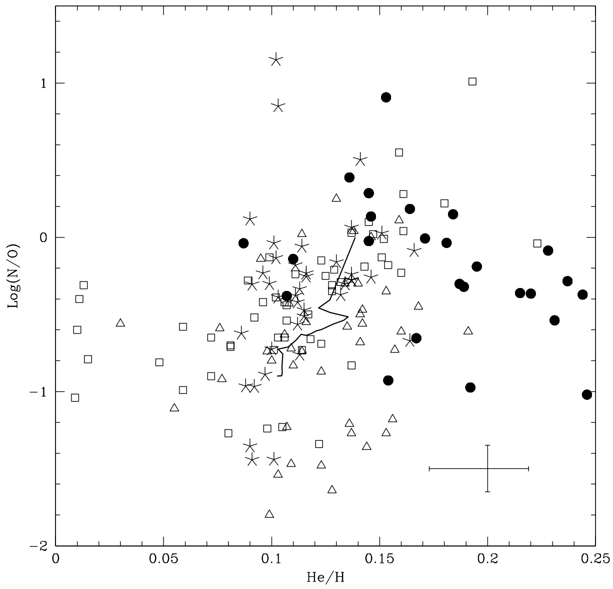

Fig. 5. log (N/O) vs. log (He/H) for our sample(filled circles), planetary nebulae from Escudero & Costa (2001) (triangles) and Escudero et al. (2004) (squares), Exter et al. (2004) (stars); solid line represents a model from Marigo (2001) with solar metallicity and mixing-length parameter $\alpha = 1.68$ (see Marigo 2001 for details).

Being α-elements, the Ne/O ratio does not reflect the chemical evolution of the interstellar medium and should remain the same along the galactic bulge and disk. The mean values and dispersions are listed in Table 7.

The mean values show that symbiotic stars have a similar Ne/O ratio as the bulge PNe from Escudero et al. (2004) or disk PNe form Maciel & Köppen (1994). On the other hand, the mean Ne/O for the Exter et al. (2004) sample, which combines bulge and disk objects, is higher than the value from our sample. Within the dispersion, this is another indication that our sample contains both bulge and disk objects.

As an additional test, we included in our analysis some symbiotics that are outside of our definition of the bulge. The mean and standard deviation of Ne/O including these objects is 0.147 ± 0.027. Since we have only a few objects outside the bulge, the derived mean values are essentially the same.

As a follow-up project we intend to observe the full sample of southern symbiotic stars to increase the statistics about physical parameters and abundances for this class of objects in different locations in the Galaxy.

Acknowledgements. This work was supported by CNPq and FAPESP. G.J.M. Luna acknowledges CNPq for his graduate fellowship (Process 141805/2003-0). We acknowledge the comments and suggestions of the referee, which helped us to improve the final quality of this work.

References

Almog, Y., & Netzer, H. 1989, MNRAS, 238, 57
Belckzyǹski, K., Mikolajewska, J., Munari, U., Ivison, R. J., & Friedjung, M. 2000, A&AS, 146, 407
Cardelli, J., Clayton, G., & Mathis, J. 1989, ApJ, 345, 245
Clegg, R. E. S. 1987, MNRAS, 229,31
Costa, R. D. D., & de Freitas Pacheco, J. A. 1994, A&A, 285, 998
Cuisinier, F., Acker, A., & Köppen, J. 1996, A&A, 307, 215
Deuel, W., & Nussbaumer, H. 1984, in ed. E. Rolfe, & B. Battrick, ESA SP-218, Proc. 4th Europeam IUE Conference, 399
Escudero, A. V., & Costa, R. D. D. 2001, A&A, 380, 300
Escudero, A. V., Costa, R. D. D., & Maciel, W. J. 2004, A&A, 414, 211
Exter, K. M., Barlow, M. J., & Walton, N. A. 2004, MNRAS, 349, 1291
de Freitas Pacheco, J. A., & Costa, R. D. D. 1992, A&A, 257, 619
Gutierrez-Moreno, A., Moreno, H., & Feibelman, W. A. 1992, ApJ, 395, 295
Gutierrez Moreno, A., & Moreno, H. 1996, PASP, 108, 972
Gutierrez Moreno, A., & Moreno, H. 1999, PASP, 111, 571
Kingdon, J., & Ferland, G. J. 1995, ApJ, 442, 714
Maciel, W. J., & Köppen, J. 1994, A&A, 282, 436
Marigo, P. 2001, A&A, 370,194
Medina Tanco, G. A., & Steiner, J. E. 1995, AJ, 109, 1770
Michalitsianos, A. G., Feibelman, W. A., Hobbs, R. W., & Kafatos, M. 1982, ApJ, 253, 735
Mikolajewska, J., Acker, A., & Stenholm, B. 1997, A&A, 327, 191
Munari, U., & Buson, L. M. 1993, MNRAS, 263, 267
Munari, U., & Buson, L. M. 1994, A&A, 287, 87
Netzer, H. 1975, MNRAS, 171, 395
Nussbaumer, H., Schmid, H. M., Vogel, M., & Schild, H. 1988, A&A, 198, 179
Pereira, C. B. 1995, A&AS, 11, 471
Pereira, C. B., Landaberry, S. J. C., & Junqueira, S. 1998, A&A, 333, 658
Pereira, C. B., Franco, C. S., & de Araújo, F. X. 2002, A&A, 385, 900
Osterbrock, D. E. 1989, Astrophysics of Gaseous Nebulae and Active Galactic Nuclei (Mill Valley, CA: University Science Books)
Schmid, H. M., & Nussbaumer, H. 1993, A&A, 268, 159
Schmid, H. M., & Schild, H. 1990, MNRAS, 246, 84
Shaw, R. A., & Dufour, R. J. 1994, ASP Conf. Ser., 61,327
Simon, V. 2003, A&A, 406, 613
Stauffer, J. R. 1984, ApJ, 280, 695
Willson, L. A., Wallerstein, G., Brugel, E. W., & Stencel, R. E. 1984, A&A, 133, 154

Online Material

Article published by EDP Sciences and available at http://www.edpsciences.org/aa or http://dx.doi.org/10.1051/0004-6361:20041994

Table 2. Reddening-corrected line fluxes (Hβ = 100)

Source/Ion	Hλ3835	NeIIIλ3869	NeIIIλ3968	Hδ	Hγ	OIIIλ4363	NIIIλ4640	HeIIλ4686	ArIIIλ4711	ArIVλ4740	Hβ	FeVIIλ4893	FeVIIλ4942	FeVIλ4872	FeVIIλ4988
CLSco	8.5	34.6	29.2	29.1	49	40.1	8.4	14.6	2.6	0	100	0	0	0	0
FNSgr	5.1	7.1	17.2	27.4	76.1	9.5	16.8	94.5	9.8	0	100	5.5	17.8	0	1.6
H2-38	0	78.2	35.2	16.4	87.3	113.2	8.8	78.5	3.5	0	100	4	9.3	0	0
Hen2-171	2.6	49.8	31.2	22.7	45	44.6	7.2	85.3	6.1	2.6	100	6.8	21.3	0	0
RTSer	0	0	12.2	20.9	44.3	7.8	0	118.8	1.4	0	100	0	0	0	0
V2416Sgr	0	1.4	0.1	08.3	28.1	4.3	17.1	80.1	0	0	100	1.8	10.5	0	0
V343Ser	0	0	0.2	20.7	39	2.8	28.1	49.4	5.4	0	100	0	10.1	0	0
V4018Sgr	14.6	3.3	19.2	25.4	44.8	6.5	0	49.2	3.4	0	100	0	7	0	0
AEAra	9.0	15.8	24.3	32.4	43.6	15.4	14.1	14.8	2.2	0	100	0	6.6	0	0
H2-5	0	0	0	20.4	41.2	24.1	0	101.7	0	0	100	0	0	0	0
AS210	5.4	12.5	18.2	24.4	44.5	16.8	0.6	67.1	1.1	0.2	100	1.7	4.3	0	1.3
Ap1-8	0	0	7.1	29.4	41.8	1.7	14	78	0	0	100	0	8.1	0	0.6
AS255	0	0	7.3	25.2	41	1.8	0	106.4	3.5	3.9	100	0	0	0	0
H1-36	6.6	110.4	42.2	32.4	65.1	52	3.2	61.9	0	9.2	100	1.5	0	0	0
YCra	0	17.9	25.3	71.5	81.5	23.4	18.8	19.8	0	8.1	100	0	0	0	0
H1-25	0	0	0	0	40.2	21.1	0	40.4	0	0	100	0	3.5	0	0
AS269	0	0	0	0	37.2	56.5	0	0	0	5.3	100	0	5.2	0	0
HKSco	9.2	1.6	15.2	24.4	35.6	4.5	7.2	101.2	10.7	6.4	100	0	4.7	0	1.7
Hen3-1342	0	0	16.2	23.4	04.6	1.4	8.4	61	3.1	0	100	0.4	4.5	0	1.9
MWC960	4.4	0	11.2	21.4	43.1	2.1	0	70.3	2.7	1.9	100	2.3	2.8	0	0
V2601Sgr	0	5.3	14.2	25.4	33.1	4.6	7.6	28.4	5.4	0	100	0	8	0	0
V3804Sgr	0	25.4	25.3	73.4	01.6	15.1	32	16.2	0	0	100	0	0	0	0
Pt1	0	0	11.2	23.4	30.2	5.5	0	59.5	0	0	100	0	0	0	0
SS73-96	0	4.9	9.1	28.3	48.9	17.3	5.4	100.2	9.5	3	100	6.3	15.6	0	0
V4141Sgr	9.9	18.6	17.2	40.4	81.7	26.6	16.4	6.9	0	1	100	0	0	0	0
H2-34	0	0	12.2	61.3	66.8	20	50.1	40.7	0	2.1	100	0	4.6	0	0
MaC1-9	0	0	14.1	09.4	40.5	6.5	0	7.8	1.3	0	100	0	0	0	0
SS73-122	4.4	16.5	11.2	66.3	68.6	23	18.5	55.3	7.5	0	100	2.9	7.7	0	0
SS73-129	0	0	12.2	31.4	71.8	8.4	0	39.6	7.7	0	100	0	0	0	0
HD319167	5.0	10.6	14.2	33.4	70.3	12.9	1.4	10.1	0	0.3	100	0	0	0	0
SS73-71	0	18.8	8.3	16.4	21.3	11.9	7.8	43.6	0	1	100	0	0	0	0
Hen3-1591	0	80.2	52.3	59.4	89.9	118.7	0	33.7	13.6	10.9	100	0	0	0	0
CD-43-14304	0	3.3	12.2	21.4	03.6	8.3	0	68.2	4.7	1.2	100	0	0	0	0
Hen3-1761	0	32.9	22.3	02.5	04.2	35.7	0	55.8	0	0	100	0	0	0	0
RRTel	11.3	45.5	34.3	91.4	38.3	33.9	3.8	86	11	0	100	5.3	22.8	0	6.8
Th3-29	0	0	0	0	45	28.8	0	9.5	0	0	100	0	0	0	0
V919Sgr	0	13.7	21.2	08.4	88.3	17.9	0	47.2	4.7	0	100	0	0	0	0
ALS2	0	11.2	12.3	71.5	62.7	7.7	0	57.7	0	6.7	100	0	0	0	0
Hen2-379	0	0	44.4	41.3	49.3	35.5	0	9.5	0	0	100	0	0	0	0
Hen3-1410	0	0	0	0	43.1	12.9	0	54.7	0	0	100	0	0	0	0
Hen3-863	0	1.5	13.3	50.4	79.9	13.3	0	59.4	7.8	2.5	100	0	0	0	0
LTDel	0	0	12.2	81.4	08.3	4.7	0	22.9	0	0	100	0	0	0	0
WRAY16377	0	6.9	11.4	49.4	04.1	14.7	0	9.4	0	0	100	0	0	0	0
K66	0	0	0	07.3	20.8	14.3	0	37.6	0	0	100	0	0	0	0
SS73-29	0	0	22.2	70.4	85.2	4.1	0	142.7	0	0	100	0	0	0	0
UUSer	0	0	14.2	24.4	41.7	3.5	0	54.9	2.7	0	100	0	0	0	0
V2506Sgr	0	0	8.2	94.5	40	0	0	59.1	0	0	100	0	0	0	0
AGPeg	6.1	2.9	14.2	97.9	46	13.9	0	100.1	5.2	0	100	0	0	0	0
AS327	0	0	11.2	21.4	43.2	5.7	0	95.6	6.1	0	100	0	0	0	0
FGSer	0	5.9	12.2	66.4	06.7	15.1	0	59.6	7.1	0	100	0	0	0	0
M1-21	0	0	10.2	91.4	52.3	0	10.8	46.2	2.5	0.4	100	0	0	0	0
PUVul	8.6	62.2	35.2	18.4	87.3	30.2	10.2	72.7	12.9	0	100	0	4.6	0	0
SS73-141	0	0	2	01.4	66.3	0	0	0	0	0	100	0	0	0	0
V2756Sgr	0	0	14.3	60.8	44	18.2	35.8	82	6.6	0	100	0	0	0	0
V2905Sgr	0	15.3	18.2	95.1	46	28.6	0	6.9	0	0	100	0	0	0	0

Source/Ion	OIIIλ4959	OIIIλ5007	FeIIλ4923	FeVIλ5146	FeVIIλ5159	FeVIλ5176	NIλ5200	FeIIλ5261	λ5270+λ5277	FeVIλ5334	λ5411+λ5424	FeIIλ5649
CLSco	15.8	51.5	5.6	0.7	1.1	0.8	1.9	0	0	0	1.6	0
FNSgr	2.7	8.5	11.7	0	2.5	0.2	0.9	0	1.8	0	0	1.8
H2-38	137.6	417.5	5.9	2.1	8	4.5	0	3.1	8.7	2	0	0
Hen2-171	113.5	336.4	0	5.4	8.5	11	0	0	0	1.4	0	0
RTSer	1	3.1	0	0	4.6	0	0.1	1.5	0	0	9.5	0
V2416Sgr	1.5	4.5	5.6	1.5	4	0	0	2.3	0	2.6	0	0
V343Ser	2.2	6.7	15.4	0	0	0	0	2.3	0	1.4	6.1	0
V4018Sgr	2.2	8.3	14.4	1	2.6	0	0.6	0	0	0.8	0	0
AEAra	10.2	29.8	14.9	0	0	0	0	0	0	0	0	0
H2-5	11.4	34.9	0	0	4.8	0	0	0	0	0	0	0
AS210	31.3	93.6	0.5	0.6	1.8	1.4	0	0.6	0	0.7	0	0
Ap1-8	3	8.9	11.4	0.4	1.7	0	0	1	0	0.3	0	0
AS255	0	0	0	0	0	0	0	6.2	0	0	0	0
H1-36	494.5	1492.7	0	1.4	2	1.8	0	0	0	1	0	0
YCra	13.2	40.8	32.6	0	4.9	0	0	0	0	0	0	0
H1-25	15.5	43.9	3.8	0	0	0	0	0	0	1.8	0	0
AS269	2.8	7.7	7.3	0	0	0	0	2.9	0	2.2	0	0
HKSco	1.8	5.4	25.1	1	1.7	0	0	0	0	0	0	0
Hen3-1342	3.5	11	10.8	0	0	0	0	0	0	0	0	0
MWC960	1.3	4	6.9	0	0	0	0	0	0	0	0	0
V2601Sgr	2.1	6.4	23.5	0	0	0	0	0	0	0	0	0
V3804Sgr	16.1	66.6	9.4	0	0	0	0	0	0	0	0	0
Pt1	1.9	6.9	0	0	0	0	0	0	0	0	0	0
SS73-96	14.6	43.9	9.8	0	0	0	0	1.1	0	0	0	0
V4141Sgr	30.6	96.3	0	0	0	0	1.4	0	0	0	0	0
H2-34	15.3	52.8	16.4	0	0	0	3.1	0	0	0	0	0
MaC1-9	0	0	0	0	0	0	0	0	0	0	0	0
SS73-122	39.1	117.2	5.4	3.5	7.6	12.5	0	2.7	0	3.2	0	0
SS73-129	0	0	0	0	0	0	0	0	0	0	0	0
HD319167	5.6	15.7	3.2	0	0.6	0	0	0	0	0	0	0
SS73-71	12.8	36.6	11.7	0	0	0	0	0	0	0	0	0
Hen3-1591	109.3	281.2	0	0	0	0	0	0	0	0	0	0
CD-43-14304	0	0	4.5	0	1.3	0	2.1	1.1	1.4	0	0	0
Hen3-1761	41.3	57.1	92.2	0	0	0	0	4.4	0	0	0	0
RRTel	55.7	155.2	0	3.6	7.8	5.7	0	0	0	1.3	9.5	0
Th3-29	11.3	39.6	0	0	0	0	0	0	0	0	0	0
V919Sgr	4.2	12.7	0	0	4.3	2.5	3.4	0	0	2	0	0
ALS2	0	2.2	8.9	0	4.5	0	0	0	0	0	0	0
Hen2-379	0	0	0	0	0	0	0	0	0	0	0	0
Hen3-1410	10.2	40.5	8.9	0	0	0	0	0	0	0	0	0
Hen3-863	0	0	15.7	0	0	0	10.9	0	0	0	0	0
LTDel	0.2	0.7	15.4	0	0	0	0	0	0	0	0	0
WRAY16377	11.5	20.6	10.8	0	0	0	0	0	0	0	0	0
K66	20.1	61.2	3.6	0	0	0	0	0	0	0	0	0
SS73-29	0	7.8	0	0	0	0	0	0	0	0	0	0
UUSer	2	6.1	12.9	0	0	0	1.1	0	1.9	0	0	0
V2506Sgr	0	0	0	0	0	0	0	0	0	0	0	0
AGPeg	0	0	7.9	0	0	0	5.2	0	0	0	0	0
AS327	0	0	5.6	0	0	0	0	0	0	0	0	0
FGSer	5.6	17.1	7.6	0	0	0	0	0	0	0	0	0
M1-21	0	0	5.8	0	0	0	0	0	0	0	0	0
PUVul	24.6	57.2	3.5	6.5	5.2	10.7	0.5	0	0	2.2	0	0
SS73-141	0	0	10.8	0	0	0	0	0	0	0	0	0
V2756Sgr	12.4	50.1	14.7	0	0	0	2.1	0	0	0	0	0
V2905Sgr	13.2	36.7	0	0	0	0	0	0	0	0	0	0

Source/Ion	FeVIIλ5721	NIIλ5755	HeIλ5876	CIVλ5801	FeVIIλ6086	OIλ6300	SIIIλ6312	OIλ6364	ArVλ6435	NIIλ6548	Hα
CLSco	0	2.1	19.6	3.9	0	0.5	0.8	0	1	0	420.1
FNSgr	2.2	4.1	17.7	6	3.6	0	1.3	0	2.5	0	353.9
H2-38	20.4	3.6	21.1	3.2	32	14.3	4.3	0	2.8	3.9	962.1
Hen2-171	55.4	7.8	9.8	0	87.2	8.9	7.1	0	4.1	26.4	345
RTSer	4.6	1.5	13.6	5.4	6.4	4.5	1.4	0	0	0	516.5
V2416Sgr	9.3	0.8	11.8	0	13.4	3.3	2	0	1.8	0	548.7
V343Ser	3.1	0.4	33.9	4.2	4.4	0	0	0	2.2	0	452.9
V4018Sgr	9.7	1.9	20.4	7.2	14.3	0	0	0	1.5	0	866.4
AEAra	0	1	23.1	5.7	0	1	1.4	1.2	5	0	898.5
H2-5	8.2	0	33.5	6.9	10.5	4.3	2.2	0	2.8	0	929.8
AS210	8.6	0.7	4.5	0.2	11.1	2.2	1.6	0	0.6	1.3	375.4
Ap1-8	4.1	1.5	16.2	2.5	5.7	0	0	0	0.5	0	854.1
AS255	0	0	27	0	0	3.8	0	0	0	0	451.4
H1-36	5.6	9.6	8.8	0	9	32	9.3	0	0	29.4	331
YCra	0	0	22	6.8	0	5.9	4	0	0	0	641.3
H1-25	3	0	9.4	0	3.6	3.4	0	0	0	3.4	458.3
AS269	0	0	6.9	0	0	9.6	0.6	0	0.3	0	330.5
HKSco	3.1	4.7	14.2	6.3	3	0	0	0	2.6	0	425.4
Hen3-1342	0	0	26	0	0	2.4	4.7	4	1.3	0	868.7
MWC960	0	1.1	20.1	0	0	1.6	1.7	1.5	0.9	0	885.7
V2601Sgr	0	3	19.6	6.4	0	0.8	2.8	0	4	0	874.8
V3804Sgr	0.8	1.7	30.4	2.2	1.2	2.4	3.2	2.9	3.3	0	896.7
Pt1	0	2.8	27.2	0	0	0	0	3.5	3	0	467.8
SS73-96	21.8	3.2	15.1	0	0	1.2	3.2	0	2.8	0	471.7
V4141Sgr	0	1.7	26.1	0	0	1.9	1.6	0	0.9	0	476.5
H2-34	7	1	35	0	11.9	2.8	4.1	0	1.6	0	516.8
MaC1-9	0	2.1	22.3	0	0	0	0	0	0	0	876.2
SS73-122	22	3.9	24.1	1.1	35.4	5.2	3.8	0	3.3	0	489.6
SS73-129	0	0	24.8	0	0	0	0	0	0	0	855.1
HD319167	0	0.3	14.3	0.6	0	0.6	0.1	0	0.4	0	897.5
SS73-71	0	1.8	27.2	1.8	6.7	2	1.7	0	3.6	0	589
Hen3-1591	0	0	72.5	0	0	13	3.7	8.3	0	7.6	674
CD-43-14304	1.3	0.3	21.5	0	0	0	0	0	0	0	845.8
Hen3-1761	0	30.8	44.8	34.7	0	0	0	0	0	0	843.1
RRTel	34.3	2	5.6	0	55.3	5.1	2.1	1.6	1.9	2.3	129.7
Th3-29	0	0	33.6	0	0	4.2	0	0	0	0	667.5
V919Sgr	0	6.6	23.1	20.3	3.6	0	0	0	0	0	499
ALS2	0	16.8	18.7	0	0	0	0	0	0	0	824.3
Hen2-379	0	0	30.6	0	0	0	0	0	0	125.4	590.6
Hen3-1410	0	1.4	28.5	0	15.1	0	0	0	1.5	0	465.8
Hen3-863	0	0	18.4	0	0	0	0	0	0	0	412.1
LTDel	0	2.9	20.4	0	0	0	0	0	0	0	253.2
WRAY16377	0	1.1	22.6	0	0	0	0	0	0	0	803.9
K66	3.7	1.4	24.6	0	4.9	4.3	1.3	1.4	0.7	0	524.2
SS73-29	26	0.2	0	0	36.2	0	0	0	0	0	257.5
UUSer	2.6	1.2	15.7	3.3	3.8	0	0	0	0	0	380
V2506Sgr	0	0	11.1	4.2	0	0	0	0	0	0	866.5
AGPeg	7.5	6.9	22.2	10.8	6.9	0	0	0	0	0	419.9
AS327	0	3.1	26	6.5	0	0	0	0	0	0	896.6
FGSer	16.8	13.7	31.7	22	15.2	0	0	0	0	0	591.5
M1-21	3	0	14.6	0	4.2	0.8	0.6	0	0.7	0	898.5
PUVul	13.4	5.7	14.7	1	22	3.1	2	1.1	1.5	0	427.6
SS73-141	0	0	11.5	3.9	0	1.7	0	0	1.1	0	309
V2756Sgr	3.5	0.9	28.8	2.4	3.6	0.7	0	0	1.3	0	466.5
V2905Sgr	0	0	28.5	12.5	2.5	0	0	0	0	0	864.6

Source/Ion	NIIλ6583	HeIλ6678	SIIλ6716	SIIλ6731	λ6717+31	ArVλ7006	HeIλ7065	ArIIIλ7135	FeIIλ7155	ArIVλ7170	ArIVλ7237	ArIVλ7262	OIIλ7320+30
CLSco	0	8.1	0	0	0	0	12.2	0.4	1.4	0.8	0	0	0
FNSgr	0	19.9	0	0	0	0	13.6	0	0	0	0	0	2.5
H2-38	11.8	5.5	0	0	0	0	10.4	3.2	2.7	2	0	1.5	7.6
Hen2-171	66.7	3	3.3	6.1	9.5	7.9	5.1	11.8	1	2.1	0.9	0.9	5.2
RTSer	0	3.3	0	0	0	0	3.7	0	0	0	0	0	0
V2416Sgr	0	5.2	0	0	0	0	5.3	0	0	0	0	0	0.1
V343Ser	0	24.3	0	0	0	0	17.1	0	0	0	0	0	0.2
V4018Sgr	0	26.6	0	0	0	0	13.5	0	0	0	0	0	0.8
AEAra	0	20.1	0	0.2	0	0	19.4	0	0	0	0	0	6.2
H2-5	0	8.7	0	0	0	0	10.7	0	0	0	0	0	0
AS210	2.9	1.3	0.8	0.7	1.6	1.3	2.7	1.8	2.1	0.9	0	0	1.1
Ap1-8	0	10.3	0.2	0.3	0.5	0	6.5	0.1	1.1	0.8	0	0	0
AS255	0	13.9	0	0	0	0	13.3	5.2	6.4	1.7	0	0	4.7
H1-36	87.6	2.7	3.2	6.4	9.6	7.7	4.6	23.7	0.5	1.5	0.5	0.8	22.2
YCra	0	12.8	0	0	0	0	12.4	0.3	3.1	1.1	0	0	0
H1-25	9.9	1.8	0.3	0.5	0.9	0	3.3	0.4	0.7	0.2	0	0.1	0.3
AS269	20.6	0.7	0	0	0	0	1.2	0.1	0.6	0.2	0	0	0
HKSco	0	12.2	0	1.4	0	0	8.9	0	0	0	0	0	2.9
Hen3-1342	0	15.5	1.8	0.2	1.9	0	10.9	2.6	6.6	0.4	0	0	3
MWC960	0	8.5	1	0	1	0	8.6	0	0	0	0	0	1.6
V2601Sgr	0	19.7	0	0	0	0	11.5	0	0	0	0	0	1.4
V3804Sgr	0	15.9	0.4	0.2	0.6	0	20.4	3.3	3.3	0.9	0	0	3.6
Pt1	0	34.2	1	1.1	2.1	0	11.9	0	0	0	0	0	4.6
SS73-96	0	11.3	0.8	0.5	1.3	0	5.8	0.1	1	1.1	0	0	5.1
V4141Sgr	0	10.3	0.3	0.1	0.3	0	16.3	2.2	0.6	0.8	0	0	1
H2-34	0	15.8	0.2	0.2	0.4	0	19.9	0.7	0	0	0	0	1.4
MaC1-9	0	21.1	0	0	0	0	0	0	0	0	0	0	1.3
SS73-122	0	8.5	0.1	0.3	0.4	3.1	15.8	4.2	2.3	2	0	0	4.4
SS73-129	0	19.9	0	0	0	0	0	0	0	0	0	0	6
HD319167	0	7.9	0.1	0.2	0.2	0	10.8	0.1	0.5	0.3	0	0	0.4
SS73-71	0	20.3	0	0	0	2.2	20.6	0.1	0.7	0	0	0	0
Hen3-1591	23.1	0	0	0	0	3.9	18.2	15.9	10.2	4.3	0	0	28.3
CD-43-14304	0	6.5	0	0	0	0	10	0.2	1.1	0.5	0	0	1.5
Hen3-1761	0	36.6	0	0	0	0	33.2	0	9.6	0	0	0	53.4
RRTel	6.3	2.4	0.2	0.5	0.6	4.2	4.9	4.3	1.1	2.3	0.4	0.4	8.6
Th3-29	0	20.1	0	0	0	0	19.7	0.9	2.8	1.2	0	0	2.8
V919Sgr	0	20.7	0	0	0	0	16.7	0	0	0	0	0	16.4
ALS2	0	18.5	0	0	0	0	9.3	0	0	0	0	0	9.8
Hen2-379	467.8	5.7	22.5	50.1	0	0	0	0	0	0	0	0	0
Hen3-1410	0	19.3	0	0	0	1.9	15.6	0	0	0	0	0	2.2
Hen3-863	0	17.8	0	0	0	0	12.7	0	0	0	0	0	8.9
LTDel	0	25.2	0	0	0	0	12.6	0	0	0	0	0	0
WRAY16377	0	8.9	0	0	0	0	7.3	0.3	0	0	0	0	4.4
K66	0	8.8	0	0	0	0	10.3	0.3	0.5	0.8	0	0	1.5
SS73-29	0	19.6	0	0	0	0	10.3	0.6	0	0	0	0	0
UUSer	0	10.3	0	0	0	0	7.9	0	0	0	0	0	0
V2506Sgr	0	7	0	0	0	0	3.1	0	0	0	0	0	0
AGPeg	0	18.2	0	0	0	0	14.6	0	0	0	0	0	8.8
AS327	0	12.2	0	0	0	0	13.5	0	0	0	0	0	4
FGSer	0	33.5	0	0	0	0	23.1	0	0	0	0	0	28
M1-21	0	8.5	0	0	0	0	8.1	0	0	0.4	0	0	0.7
PUVul	0	5.2	0	0	0	2.9	9.8	1.4	0.6	2.2	0	0	2.1
SS73-141	0	7.3	0	0	0	0	4.1	0	0	0	0	0	0
V2756Sgr	0	17.5	0	0	0	0	14.2	3.1	0	0	0	0	7
V2905Sgr	0	9	0	0	3.7	0	13.9	0	0	0	0	2.9	8.1